Draft version May 2, 2026
Typeset using LaTeX **twocolumn** style in AASTeX7

Speckle Interferometry at SOAR in 2024 and 2025

Andrei Tokovinin,[1] Brian D. Mason,[2] Rene A. Mendez,[3] and Edgardo Costa[3]

[1] *Cerro Tololo Inter-American Observatory — NFSs NOIRLab Casilla 603, La Serena, Chile*
[2] *U.S. Naval Observatory, 3450 Massachusetts Ave., Washington, DC, USA*
[3] *Universidad de Chile, Casilla 36-D, Santiago, Chile*

ABSTRACT

Results of speckle interferometry observations at the 4.1 m SOuthern Astrophysical Research (SOAR) telescope obtained during 2024–2025 are presented. We present 5316 measurements of relative positions and magnitude differences in 3532 pairs (including 524 unpublished measures made before 2024) with median and minimum separations of 0.″19 and 12 mas, respectively; non-resolutions of 1723 stars are documented as well. More than 400 pairs have been resolved here for the first time and not resolved by Gaia; among those are 222 TESS objects of interest, 46 inner subsystems in known wider binaries within 100 pc, and 43 subdwarfs. Positional measurements are used to compute or improve binary orbits; elements of 202 orbits with meaningful errors are given here, while preliminary and tentative orbits are published elsewhere. Of special note are orbits with large and accurately measured eccentricties (e.g. $e = 0.9866 \pm 0.0014$ for J13038−2035) and orbits of pre-main sequence binaries. Appendix contains parameters of 86 binaries used for calibration of pixel scale and orientation.

Keywords: binaries:visual

1. INTRODUCTION

Speckle interferometry replaced visual micrometer observations of double stars in the last decades of the 20th century, improving both the accuracy and the angular resolution. At that time, most speckle observations were made by the CHARA group (H. A. McAlister et al. 1993; B. D. Mason et al. 2009; B. D. Mason & W. I. Hartkopf 2026) to monitor orbital motions and to discover new close pairs. Nowadays, solid-state detectors like electron-multiplication (EM) CCDs and CMOS make this method more practical and efficient. Without being exhaustive, we can cite recent works by E. P. Horch et al. (2017, 2021), A. Mitrofanova et al. (2021), and C. A. Clark et al. (2024). Speckle instruments have been used extensively to characterize duplicity of exohosts (S. B. Howell et al. 2021; K. V. Lester et al. 2023) and to survey diverse stellar populations for companions (e.g. nearby low-mass stars, M. Janson et al. 2012; E. H. Vrijmoet et al. 2022). Speckle interferometry is by far the largest source of high-resolution astrometry of binary stars, compared to adaptive optics (A. W. Mann et al. 2019) and long-baseline interferometry (G. Torres et al. 2022). Owing to its lower spatial resolution and decade-long time span, the data from Gaia (Gaia Collaboration et al. 2016) cannot replace speckle interferometry.

This paper continues the series of double-star measurements made at the 4.1 m SOuthern Astrophysical Research (SOAR) telescope since 2008 with the speckle camera, HRCam. Previous results are published by A. Tokovinin et al. (2010b, hereafter TMH10) and in (A. Tokovinin et al. 2010a; W. I. Hartkopf et al. 2012; A. Tokovinin 2012; A. Tokovinin et al. 2014, 2015, 2016b, 2018, 2019, 2020, 2021, 2022; B. D. Mason et al. 2023; A. Tokovinin et al. 2024). Observations reported here were made during 2024–2025; we also give some unpublished observations made before 2024.

The structure and content of this paper are similar to the previous papers of this series. Section 2 reviews all speckle programs that contributed to this paper, the observing procedure, and the data reduction. The results are presented in Section 3 in the form of electronic tables archived by the journal. We also discuss new resolutions and present orbits resulting from this data set. A short summary is given in Section 4. The Appendix contains data on 86 binaries used for calibration of pixel scale and orientation.

2. OBSERVATIONS

2.1. *Observing Programs*

The observations reported here were obtained with the *high-resolution camera* (HRCam) — a fast im-

ager designed to work at the 4.1 m SOAR telescope (A. Tokovinin 2018a). It was used to execute several observing programs, some with common targets. About 10 nights per year were used, divided almost evenly between regular allocations and additional engineering time (usually morning hours on bright-Moon nights). A total of 21 individual observing runs, ranging from a few hours to two nights, were executed in 2024–2025.

The allocated time was distributed between the following projects:

- Multiple stars and orbits (3 nights, PI A.T.)
- Orbits and masses (4 nights, PI R.M.)
- Orbits of nearby M dwarfs (one night, PI E. Vrijmoet). Most observations up to 2025.1 are published by E. H. Vrijmoet et al. (2026); they are provided here for completeness. The first results of this long-term effort are published by E. H. Vrijmoet et al. (2022).
- Survey of nearby M dwarfs (two nights, PI M. Leblanc). These data (mostly non-resolutions) are not published here.
- TESS follow-up (one night of SOAR partner's time in 2024). All observations are given here and posted at the Exofop site,[4] see also C. Ziegler et al. (2020, 2021). Previously unpublished measures of resolved TESS objects of interest (TOIs) made after 2021.09 are included in our data table, see Section 3.4.

The engineering time was used to complement the scheduled programs (for example, to compensate weather and poor-seeing losses) and to observe orbital or neglected pairs. Additional details on the HRCam programs and their motivation can be found in A. Tokovinin et al. (2024). The HRCam results are eventually ingested into the Washington Double Star (WDS) database (B. D. Mason et al. 2001).

The proprietary period of the SOAR data is 18 months. To prevent loss of information, we include in the data tables the HRCam observations made in 2021–2022 for the projects led by K. Franson and B. Bowler (nearby stars with astrometric acceleration) and a search for resolved subsystems in wide binaries from the list of J. J. Andrews et al. (2017) led by J. Chanamé; we expect that these projects will publish the HRCam data and their analysis in the future. We also include here recent observations of hierarchical systems used in (A. Tokovinin 2025a,b, 2026a) and observations of doubly-eclipsing quadruples (S. R. Majewski et al. 2025).

Speckle observations with HRCam is an iterative cycle beginning with observing program preparation, selection of targets for the upcoming runs, using custom software during observations (including pointing the telescope), data processing pipeline, and archiving the results in the custom database which counts 46,113 entries as of January 1, 2026. The latest results are reflected in the program, allowing to plan next observations. This closed-loop process with a fast duty cycle is particularly suitable for monitoring fast orbital motions. Determination of orbits is a time-domain science that requires flexible and regular access to the telescope rather than standard scheduling per semester.

2.2. *Instrument*

The instrument and observing procedure are described in the previous papers of these series (e.g. A. Tokovinin et al. 2020) and briefly summarized by B. D. Mason et al. (2023). We used mostly the near-infrared I filter (824/170 nm), while the Strömgren y filter (543/22 nm) was chosen for brighter and/or closer pairs. The pixel size is 15.3 mas. In the standard observing mode, two data cubes of 200×200 pixels (3.″15 field) and 400–600 frames each are taken on each target with an exposure time of 25 ms. A single reference star is observed immediately after or before, if needed. Pairs wider that 1.″5 are observed with a 400×400 format and, optionally, with a 2×2 binning. Each data cube is used to compute the power spectrum, the high-pass filtered speckle autocorrelation function (ACF), the averge centered and the shift-and-add images.

The HRCam normally receives the light through the SOAR adaptive optics module, SAM (A. Tokovinin et al. 2016a). The SAM was removed from the telescope in January 2024 for upgrade. The HRCam was installed without SAM using a modified mechanical adaptor and tested on the engineering nights of 2024 January 26 and February 26-27. The atmospheric dispersion was compensated by the regular SOAR atmospheric dispersion corrector (ADC), instead of the SAM ADC. These tests demonstrated that HRCam can work without SAM, if needed, without affecting its performance and results. The new speckle instrument HRCam2 based on a CMOS camera will be installed at the asquisition port and will employ the SOAR ADC. HRCam2 has been tested on sky in 2026 January.

Meanwhile, the SAM was upgraded in 2024 February to SAMplus (D. M. Faes et al. 2018), including,

[4] https://exofop.ipac.caltech.edu/tess/

among other things, replacement of its deformable mirror (DM). SAMplus was tested during the March 25–26 engineering run, using HRCam as an imager. From that date on, HRCam again receives the light through SAM with its upgraded DM, and the regular SAM ADC is used. The first scheduled science night in this configuration was 2024 March 28. Differences in the instrument configuration do not affect such HRCam characteristics as sensitivity, resolution, and dynamic range.

The diffraction limit λ/D of the 4.1 m SOAR telescope in the y and I filters is 27 and 41 mas, respectively. However, many pairs at closer separations could be measured. Their positions are obtained by modeling the speckle power spectra of the target and of the reference star; they are less accurate and are marked by colons. Typical HRCam detection limits (contrast vs. separation) are illustrated in Figure 1 of A. Tokovinin et al. (2024), see also Section 3.4. The SOAR speckle instrument usually gets data on 300 targets per night, surpassing typical efficiency of speckle instruments at other telescopes by a factor of ∼5.

2.3. *Image Quality*

The signal to noise ratio in speckle interferometry strongly depends on the object flux and seeing. This relation has been explored by A. Tokovinin (2024a) using both the real HRCam data and simulations. In 2024–2025, the seeing at Cerro Tololo and Cerro Pachón was worse than usual. The median Full Width at Half Maximum (FWHM) of centered images determined by the speckle pipeline is 0.″954 for all 2024-2025 data. Among the 21 observing runs, the smallest and largest FWHM medians are 0.″83 and 1.″35, respectively. Poor seeing increases the measurement errors for faint stars. Some observing runs were affected by thin clouds (cirrus).

The size of the stellar images at SOAR is enlarged, compared to the seeing, by two effects: inhomogeneous air in the dome (dome seeing) and optical aberrations. The dome seeing causes characteristic slow and irregular distortions of the images dominated by random low-order aberrations like defocus or astigmatism; they are qualitatively different from the normal (external) seeing. Although the dome-seeing distortions are obvious in some speckle movies, presently they are not quantified. The optical aberrations, on the other hand, become apparent under very good seeing. The night of 2024 November 16/17 had excellent conditions: the seeing monitor indicated values below 0.″5 for most of the night, and the wind was slow. Yet, the median FWHM of the speckle images in this run was 0.″83. Re-tuning the SOAR optics in the middle of the night did not help much. The aberrations are revealed by the irregular shape of the average centered image derived from the data cube. For example, the image cube HI.727 taken immediately after tuning the SOAR optics yields a FWHM size of 0.″89×0.″64 (elongated horizontally) and a spotty structure, while the external seeing was better than 0.″4 (Figure 1, left). The aberrations evolve with time and telescope elevation. Occasionally, a FWHM resolution of 0.″5 is attained in one or both directions, as illustrated in Figure 1, right. Aberrations under good seeing cause systematic distortions of the speckle power spectra, hence they degrade the sensitivity and the astrometric accuracy of speckle interferometry. The observer should control the telescope focus while keeping an eye on evolving conditions and image quality.

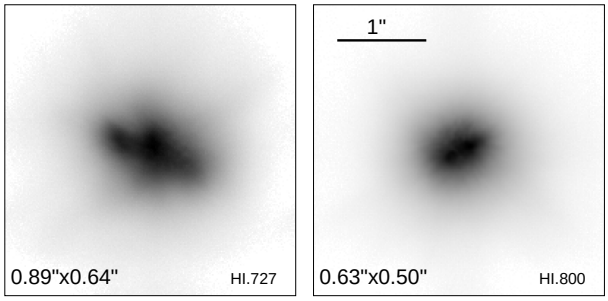

Figure 1. Mean centered images of single stars (in negative square-root rendering) recorded with HRCam on 2024 November 16/17 under excellent seeing at an elevation around 60° in the I filter. The size of each image is 3.″15. The FWHM along horizontal and vertical directions is indicated. The first image HI.727, recorded immediately after tuning the SOAR optics, shows clear signs of residual aberrations. The image HI.800 taken an hour later is sharper, although still somewhat asymmetric.

On 2024 February 26/27 and 27/28, the HRCam observations were adversely affected by the jitter of the SOAR mount. The jitter appeared and disappeared intermittently, usually at telescope elevation of 50°and below. The oscillations were quasi-periodic, with the dominant frequency between 1 Hz and 2.5 Hz. The rms motion of the star centroid without jitter is typically about 0.″3 in a 10 s data cube. The oscillations increase the rms to ∼1″or more. Motion of the star in one direction smears the speckles and strongly distorts the speckle power spectrum. The non-stationary nature of the oscillations prevents calibration of this distortion by reference stars. In one case, the oscillation was present in one data cube and stopped in the following cube taken a few seconds later on the same target. Similar oscillations with smaller amplitude were encountered in some other runs. Periodic errors of the encoders, partially amplified by the response of the mount servo, is one of the known causes of oscillations; hardware problems in the telescope mount drives is another.

2.4. *Updated Calibration and Astrometric Accuracy of HRCam*

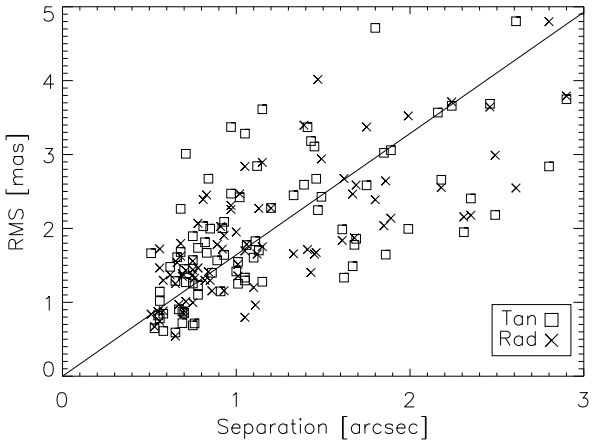

Figure 2. The rms deviations of the calibrator binaries from their models in the tangential (squares) and radial (crosses) direction vs. angular separation. The line is a linear approximation $\sigma \approx 1.64\rho$ which corresponds to the relative pixel scale accuracy of 0.16% or the position angle accuracy of 0.°09.

Calibration of the pixel scale and orientation of HRCam is based on observations of relatively wide pairs, called *calibrators* for brevity. Although the orbits of many "slow" pairs are of low quality or unknown, the small observed arcs can be accurately modeled. As the calibrator models improve with time, the accuracy of the old (published) data can be improved as well by retroactive calibration.

The set of calibrators and their models were revised iteratively several times. The previous list of 104 calibrators used the data up to 2021.75 (A. Tokovinin et al. 2022). These models were checked against Gaia data release 3 (GDR3) (Gaia Collaboration et al. 2021a), and a minor systematic error in the overall calibration was corrected from 2021 on. In 2025 the calibrator set was revised again and reduced to 86 pairs, eliminating two pairs (J01316−5322 and J18250−0135) with inner subsystems detected via wobble (A. Tokovinin 2026a) and several calibrators with magnitude differences above 3 mag.

The calibrator models (73 orbits and 13 linear) were updated here using the SOAR data till 2025.77 (see Appendix). The rms deviations σ between the data (relative positions) and the models in the tangential and radial directions are similar: their medians are 1.78 mas and 1.72 mas, respectively. The deviation increases with the separation ρ (in arcseconds) as $\sigma \approx 1.64\rho$ mas, corresponding to an accuracy of 0.16% in the pixel scale and 0.°09 in position angle (Figure 2). Comparison of the updated models with GDR3 relative positions reveals no measurable systematic differences. The GDR3 astrometry of both components is available for 48 calibrators (the rest are either unresolved by Gaia or lack 5-parameter solutions for some components, making their GDR3 relative positions unreliable). For this subset, the mean difference between the calibrator models interpolated to 2016.0 and the GDR3 positions in the relative pixel scale is $1.2\,10^{-5}$; the rms difference of 0.12% in scale is similar to the internal accuracy of our calibrator models, 0.16%. The mean difference in position angle between SOAR calibrators and GDR3 is +0.°022, the rms scatter is 0.°036, and the rms difference in the tangential direction is 1.77 mas.

Using the revised calibrator models, we can correct all SOAR speckle data retroactively to improve their accuracy. The data of some observing runs are less accurate for instrumental reasons, e.g. a detector with poor charge transfer efficiency used in 2014.75, 2014.86, and 2016.95, or problems of the SOAR Nasmyth rotator control in 2018.25. For some calibrators, a few deviant points were removed while fitting the models. We plan to publish all SOAR speckle data with these corrections in the future.

The published HRCam results contain only the internal measurement errors σ_i in the tangential and radial directions. For the data of 2024–25, the median estimated internal errors σ_i are 0.42 and 0.39 mas in the radial and tangential directions, respectively (for comparison, the median internal errors of the HRCam measures in 2023 are 0.32 mas). The external measurement error σ_e can be estimated as a quadratic sum of the internal error and the calibration uncertainty:

$$\sigma_e^2 = \sigma_i^2 + (C\rho)^2, \qquad (1)$$

where $C = 1.6$ mas/arcsec. For our data, the median separation of 0.″19 corresponds to the calibration error $C\rho$ of 0.30 mas, so for most close pairs the calibration is only a minor contributor to the astrometric errors. In fitting the orbits, measurement errors of 2 mas are usually adopted, in agreement with Figure 2; for close and bright pairs with reliable orbits the residuals of the SOAR measures are often below 1 mas.

3. RESULTS

3.1. *Data Tables*

The results (measures of resolved pairs and non-resolutions) are presented in the same format as in A. Tokovinin et al. (2024). The long tables are published electronically; here we describe their content.

In both tables, each object is identified by its WDS code based on the J2000 position (such codes are gen-

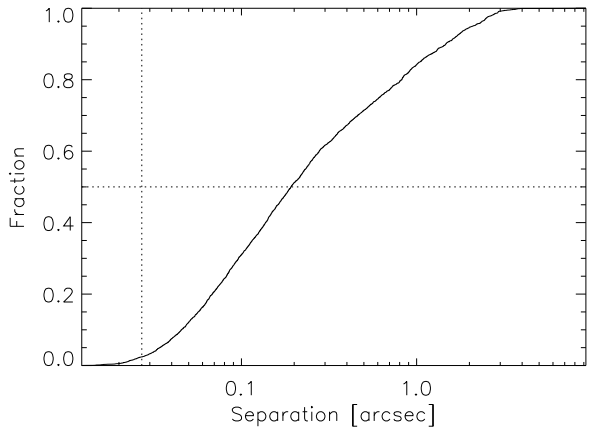

Figure 3. Cumulative distribution of angular separations in Table 1. The vertical dotted line shows the diffraction limit of 27 mas in the y filter.

erated if missing in the WDS, e.g. for single stars), discovery designation (DD), alternative name (when available), and the J2000 coordinates. The DD is a name assigned by the WDS compilers to each pair. As noted in A. Tokovinin et al. (2024), the DDs are obsolete and nowadays they are used infrequently by the astronomical community; we keep them for compatibility with the WDS. For pairs found only in the WDS supplement, WDSS,[5] the coordinate-based WDSS 14-character codes are listed instead of the DDs.

Table 1 lists 5316 measures of 3532 resolved pairs and subsystems, including new discoveries (Figure 3). Equatorial coordinates for the epoch J2000 in degrees are given in columns (4) and (5) to facilitate matching with other catalogs. Circumstances of this particular observation (Julian year, filter, number of averaged cubes), be it Table 1 or 2, are given in columns (6) through (8). In the case of resolved multiple systems, the positional measurements and their errors (columns 9–12) and magnitude differences (column 13) refer to the individual pairings between components, not to their photocenters. As in the previous papers of this series, we list the internal errors derived from the speckle power spectrum modeling and from the difference between the measures obtained from two data cubes. The real (external) errors are larger (see equation 1).

The flags in column (14) indicate the cases where the true quadrant is determined (otherwise the position angle is measured modulo 180°), when the relative photometry of wide pairs is derived from the long-exposure images (this reduces the Δm bias caused by speckle

[5] http://www.astro.gsu.edu/wds/Supplement/wdss_summ.txt

Table 1. Measurements of Double Stars at SOAR

Col.	Label	Format	Description, units
1	WDS	A10	WDS code (J2000)
2	Discov.	A16	Discoverer Designation
3	Other	A16	Alternative name
4	R.A.	F9.5	R.A. J2000 (deg)
5	Decl.	F9.5	Declination J2000 (deg)
6	Epoch	F9.4	Julian year (yr)
7	Filt.	A2	Filter
8	N	I2	Number of averaged cubes
9	θ	F8.1	Position angle (deg)
10	$\rho\sigma_\theta$	F5.1	Tangential error (mas)
11	ρ	F8.4	Separation (arcsec)
12	σ_ρ	F5.1	Radial error (mas)
13	Δm	F7.1	Magnitude difference (mag)
14	Flag	A1	Flag of magnitude difference[a]
15	Tag	A1	System tag[b]
16	$(O-C)_\theta$	F8.1	Residual in angle (deg)
17	$(O-C)_\rho$	F8.3	Residual in separation (arcsec)
18	Ref	A9	Orbit reference[c]

[a] Magnitude flags: q – the quadrant is determined; * – Δm and quadrant from average image; : – noisy data or tentative measure.

[b] System tags: A – Hipparcos-Gaia acceleration stars (K. Franson); C – Wide pairs observed for J. Chanamé; G – Wide pairs with relative positions in GDR3, likely physical; g – Wide pairs with relative positions in GDR3, likely optical; M – M-type dwarfs within 30 pc (E. H. Vrijmoet et al. 2022, 2026); N – New pair resolved in 2024–2025; P – Hierarchical systems from B. P. Powell et al. (2023); T – Hierarchies within 100 pc (A. Tokovinin 2023a); Z – TESS objects of interest (C. Ziegler et al. 2021).

[c] Orbit References are provided at https://crf.usno.navy.mil/data_products/WDS/orb6/wdsref.html

(This table is available in its entirety in machine-readable form in the online article.)

Table 2. Unresolved Stars

Col.	Label	Format	Description, units
1	WDS	A10	WDS code (J2000)
2	Discov.	A16	Discoverer Designation
3	Other	A16	Alternative name
4	R.A.	F9.5	R.A. J2000 (deg)
5	Decl.	F9.5	Declination J2000 (deg)
6	Epoch	F9.4	Julian year (yr)
7	Filt.	A2	Filter
8	N	I2	Number of averaged cubes
9	$\rho_{\min}$	F7.3	Angular resolution (arcsec)
10	$\Delta m(0.15)$	F7.2	Max. Δm at $0\farcs15$ (mag)
11	$\Delta m(1)$	F7.2	Max. Δm at $1''$(mag)

(This table is available in its entirety in machine-readable form in the online article.)

anisoplanatism), and when the data are noisy or the resolutions are tentative (see TMH10).

To facilitate identification of pairs that either have been resolved previously but remain unpublished or are published but not yet entered in the WDS, we provide in column (15) one-character tags. Their meaning and the numbers of resolved individual systems with each tag are as follows: A — acceleration stars (K. Franson, B. Bowler, $N = 51$), C – subsystems in wide pairs (J. Chanamé, $N = 16$), G or g — wide pairs with relative positions in GDR3 (121 and 78, respectively), M – nearby M-type stars (E. H. Vrijmoet et al. 2022, 2026, $N = 8$), N — new pairs resolved here for the first time (Section 3.5, $N = 353$), P — hierarchical systems published by B. P. Powell et al. (2023, $N = 10$), T — components of triple or higher-order hierarchies within 100 pc (A. Tokovinin 2023a, $N = 18$), Z — TESS objects of interest (C. Ziegler et al. 2021, $N = 2$).

For binary stars with known orbits, the residuals to the latest orbit (see Section 3.6) and its reference are provided in columns (16)–(18). Residuals close to 180° mean that the orbit swaps the brighter (A) and fainter (B) stars. However, in some binaries or triples the secondary is fainter in one filter and brighter in other. In these cases, it is better to keep the historical identification of the components in agreement with the orbit and to assign a negative magnitude difference Δm.

The non-resolutions of 1723 targets (mostly reference stars) are reported in Table 2. Its first columns (1) to (8) have the same meaning and format as in Table 1. Column (9) gives the minimum resolvable separation when pairs with $\Delta m < 1$ mag are detectable. It is computed from the maximum spatial frequency of the useful signal in the power spectrum and is normally close to the formal diffraction limit λ/D. The following columns (10) and (11) provide the indicative dynamic range, i.e., the maximum magnitude difference at separations of 0.″15 and 1″, respectively, at 5σ detection level.

3.2. *Nearby Hierarchical Systems*

Monitoring orbital motions in nearby resolved multiple systems is the core of the SOAR speckle program. Accumulation of the data defines the inner and outer orbits, thus constraining the dynamical state of these hierarchical systems. Statistics of mutual inclinations, period ratios, and masses can be compared to the predictions of various formation scenarios. It is already clear that hierarchies in the field originate from different formation channels, but their relative role and its dependence on the environment and stellar mass are debated (A. Tokovinin 2021). Recent observational work

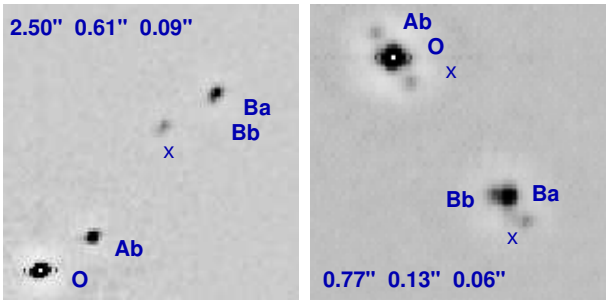

Figure 4. Fragments of speckle ACFs of two new 2+2 quadruples, in negative rendering. The orientation is standard (north up, east left). The components corresponding to specific peaks are marked, with the ACF center marked by O and by a white dot. Peaks corresponding to cross-correlations between secondaries, e.g. Ba,Ab, are marked by 'x' (ACF of a resolved quadruple has 12 secondary peaks). The outer and two inner separations are indicated.

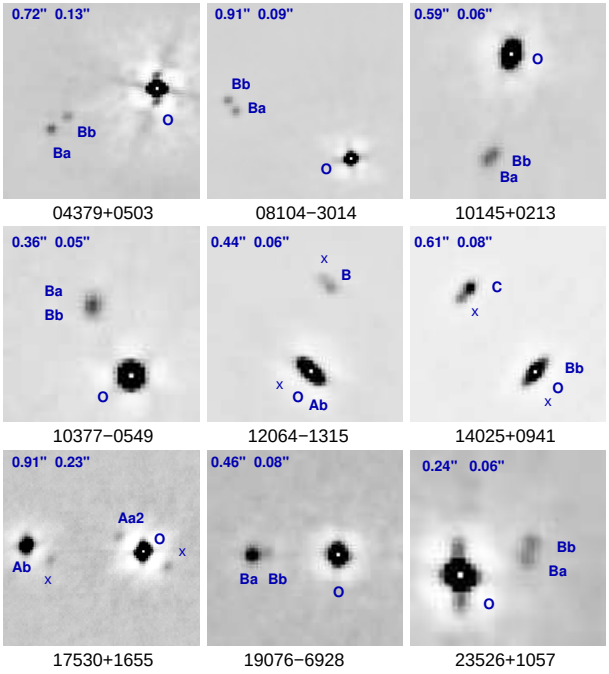

Figure 5. Speckle ACFs of 9 new close triples with sub-arcsecond outer separations and separation ratios above 1:10.

based on the SOAR data is published in (A. Tokovinin 2023b, 2025a, 2026a,b). For some stars, speckle interferometry is combined with radial velocities (A. Tokovinin 2023c, 2025b). Speckle interferometry was also used by Z. D. Hartman et al. (2025) to resolve inner subsystems in wide binaries. R. A. Mendez et al. (2025) characterized several compact hierarchies with the Gemini 8 m telescope. Very tight subsystems are resolved by interferometers such as CHARA (e.g. G. Torres et al. 2022).

The SOAR angular resolution, 0.″03, together with the third Kepler law, mean that periods short enough to be measurable on the human lifetime scale are limited to relatively nearby stars: at a distance of 100 pc, the resolution limit of 3 au corresponds to decade-long periods, while wider pairs move more slowly. So, the most interesting targets are nearby binaries and triples. Our attention is focused on stars within 100 pc. Over a thousand new candidate hierarchies in this volume were identified in the Gaia catalog of nearby stars, GCNS (Gaia Collaboration et al. 2021b) as source pairs with common distance and proper motion (PM) where at least one star had signs of inner subsystems such as an increased reduced unit weight error (RUWE) or multi-peak transits; ∼500 inner subsystems in these hierarchies were resolved at SOAR in 2022–2023 (A. Tokovinin 2023a). Periods of the closest subsystems range from years to decades, and their fast orbital motion is being monitored at SOAR. In 2024–2025, we measured 357 such targets. One of those, WDS J13038−3645, is not confirmed and appears to be spurious.

Many interesting hierarchies have been discovered at SOAR accidentally when previously known binaries from the WDS in need of modern measures were targeted. This led us to the idea of observing all WDS pairs within 100 pc that lack previous SOAR data, in hope of discovering new hierarchies. Note that many binaries and triples with components of comparable masses are missing from the GCNS because Gaia did not determine their parallaxes. Only systems with substantial contrast or very small separations where single-star astrometric solutions were accepted by Gaia are considered here. We selected from the GCNS stars brighter than $G = 13$ mag south of declination +20°whose position matches WDS pairs with separations under 3″. These criteria are dictated by the capabilities of HRCam. In this sample, there are 1927 WDS pairs that lack any HRCam data. A subset of 401 most promising pairs from this list with RUWE above 1.4 was included in the observing program, and 375 of those were observed as "fillers" in the general speckle program.

The first results of this effort are encouraging. Thirty five new triples and two quadruples were discovered (a 10% "success rate"); they are listed in Table 3. Some of those were confirmed by subsequent SOAR observations. The new inner pairs were resolved in 20 secondary and 19 primary components. Figure 4 illustrates the two new quadruples, while Figure 5 shows nine new compact triples with comparable separations identified in this project. It is noteworthy that some outer pairs were discovered in the 21st century using adaptive optics or speckle interferometry, but their inner subsystems have been missed. Of particular interest are so-called double twins, were faint secondaries are actually pairs of similar low-mass stars. Such hierarchies often have comparable inner and outer separations and approximately coplanar low-eccentricity orbits, like the emblematic low-mass triple system LHS 1070 (A. Tokovinin 2018b). Many inner subsystems in the new hierarchies have short estimated periods, and their orbits can be determined (if the monitoring at SOAR continues) to probe the internal dynamics. In WDS J19540+1518 (STF 2596), orbit of the inner pair Aa,Ab with a period of 68 yr was derived from the wobble in the archival measures; the faint star Ab turned out to be as massive as Aa and was revealed

Table 3. New Resolved Triples Within 100 pc

WDS	Comp.	ρ_{out} (″)	ρ_{in} (″)	Δm_{in} (mag)	DD
00049−3230	Aa,B	1.32	0.060	0.3	SEE 500
00581−5742	Aa,B	0.89	0.081	2.6	B 1027
02195−3137	Aa,B	1.70	0.095	2.4	KPP2848
03232−1404	Aa1,Ab	2.50	0.614	1.0	DAM1303
03232−1404	Aa,Ab1	2.50	0.085	0.6	DAM1303
03552+0417	A,Ba	1.36	0.149	0.1	A 2349
04173+1214	Aa,B	0.71	0.049	0.4	RAO 544
04379+0503	A,Ba	0.73	0.135	0.4	ELP 10
05089−1255	A,Ba	1.50	0.154	0.2	RST3413
05130−7028	Aa,B	1.69	0.079	0.0	JNN 32
05496−1429	A,Ba	2.31	0.141	1.9	BU 94
07494−3033	A,Ba	1.53	0.237	3.6	I 186
08104−3014	A,Ba	0.91	0.094	0.0	I 791
09002+1550	A,Ba	1.93	0.163	2.9	ALD 115
10145+0213	A,Ba	0.59	0.059	0.1	RAO 572
10377−0549	A,Ba	0.36	0.051	0.0	JNN 73
12064−1315	Aa,B	0.44	0.058	0.5	JNN 77
12153−3204	Aa1,Ab	1.53	0.076	0.6	LDS4197
12203−5242	Aa,B	2.58	0.149	1.7	BRT2072
14025+0941	Ba,C	0.61	0.078	0.6	RAO 309
14306+0306	A,Ba	2.56	0.433	0.0	RAO 588
14562+1745	A,Ca	1.90	0.047	0.1	GII 61
16254−2710	A,Ba	2.92	0.335	1.9	LDS4666
16270−6944	A,Ba	1.97	0.221	0.52	NSN 351
16535−6049	Aa,B	1.81	0.059	1.4	B 2396
17080−1929	Aa,B	2.47	0.040	0.7	NSN 139
17530+1655	Aa1,Ab	0.91	0.227	3.3	CRC 27
18133+0752	Aa,B	0.77	0.128	1.2	RAO 606
18133+0752	A,Ba	0.77	0.062	0.9	RAO 606
18574−3352	A,BC	2.39	0.330	0.8	B 956
19076−6928	A,Ba	0.46	0.083	1.7	TDT1240
19252+0227	A,Ba	1.95	0.106	3.1	STF2513
19344−7657	Aa,B	2.19	0.228	0.8	KPP4155
19475−2150	A,Ba	1.37	0.133	2.6	STN 49
19540+1518	Aa,B	2.22	0.090	3.0	STF2596
19552−0051	Aa,B	1.96	0.108	0.1	BU 830
23097−0158	Aa,B	1.66	0.045	0.6	CRC 76
23414−0838	A,Ba	1.75	0.130	2.0	A 423
23526+1057	A,Ba	0.24	0.058	0.1	YSC 17

as an eclipsing pair; so, this classical visual binary is in fact a quadruple system (A. Tokovinin 2026a).

The majority of candidate triples identified by the elevated RUWE remained unresolved. Some of those are real triples where the inner companions are too close and/or too faint for speckle resolution. In some other cases, the RUWE could be increased by the orbital motion in the wide pairs or by occasional blending of their components in Gaia. Close nearby pairs have an elevated RUWE caused by their relatively fast orbital motion. Measurements at SOAR, combined with the existing data, can define their orbits. Several first-time orbits were derived from single SOAR measures of neglected pairs within 100 pc. However, most these orbits are preliminary owing to scarce or inaccurate historic data.

3.3. *New Metal-poor Binaries*

In 2025 we started monitoring nearby metal-poor stars with the purpose of creating a sizable sample of local Galactic halo binaries. This effort extends our long-term program on securing data for the mass-luminosity-metallicity relation, MLR (R. A. Mendez et al. 2021). A comparison of empirical masses derived from visual orbits with stellar evolutionary models can be found in Figure 10 of E. P. Horch et al. (2015); see also an update in E. P. Horch et al. (2019). Their analysis, however, compares masses with colors which are affected by line-blanketing (selective absorption by spectral lines). We plan to use luminosities, as in A. W. Mann et al. (2019). Our calculation of the theoretical MLR using MESA isochrones indicates that for these objects, near-IR photometry is rather insensitive to metallicity effects, a fact that A. W. Mann et al. (2019) indeed point out (see their Figure 16). Instead, optical photometry should be used, also extending the metalliciy range to [Fe/H] < -0.5. We furthermore note that the MLR analysis should be restricted to objects on the main sequence, which for the age of the Halo implies masses of less than about 0.85 $\mathcal{M}_\odot$.

In order to have the best chance to resolve metal-poor stars, we constrained our sample to objects closer than 100 pc, selected from the GCNS (Gaia Collaboration et al. 2021b). This catalog, which is based on GDR3, does not give metallicities directly, but a cross match with the general GDR3 catalog does provide such information. The metallicities in GDR3 are determined from the on-board Blue (BP) and Red (RP) prism photometers which collect low resolution spectrophotometric measurements of spectral energy distributions over the wavelength ranges 330-680 nm and 630–1050 nm, respectively; and from the radial velocity spectrometer (RVS) which collects medium resolution ($R \sim 11700$) spectra over the wavelength range 845–872 nm centered on the Calcium triplet region (Gaia Collaboration et al. 2016; A. Recio-Blanco et al. 2023; R. Andrae et al. 2023). These metallicities are limited to objects brighter than $G = 12$ mag (D. Katz et al. 2023), which is a good match to the HRCam magnitude limit. Eventually one could also crossmatch with other suitable spectroscopic catalogs to further enlarge the sample with measured metallicities.

The GCNS has over 330,000 entries. For a local halo normalization of 1%, one would expect to have over 3000 local subdwarfs. If roughly half of them are in binary systems (as for the disk stars, D. Raghavan et al. 2010) then the sample of Galactic halo binaries would be around 1500 pairs over the whole sky. We can improve the binary detection rate by observing only those objects that have some indication of binarity in the Gaia catalog, particularly the RUWE (L. Lindegren et al. 2021), and the `ipd_frac_multi_peak` (Z. Penoyre et al. 2022; Gaia Collaboration et al. 2021a), and also the F2 goodness-of-fit parameter in the Hipparcos catalog [6]. Based on these constrains, we selected low-metallicity binary candidates ([Fe/H] < -1.2 dex) with $V < 12$ or $G < 11.5$ mag and negative declination. After discarding already known binaries listed in the WDS, we ended up with 87 targets, all of which were observed. Out of these, 43 pairs (including triples) were resolved (tag N in Table 1), with another 8 wider pairs also found in GDR3 (tags G or g). The selection of binary candidates using GDR3 is therefore very efficient, leading to a "success rate" over 50%.

The closest new pairs are expected to move fast, so their orbits can be determined within several years, leading eventually to the measurement of masses. For example, the estimated period of J02270−0326 is ∼7 yr. Interestingly, five subdwarfs are revealed as triples: J01483−7004 (Aab-B, 0.″065 and 0.″51), J01516−3757 (0.″45 and 0.″71, trapezium-like), J03258−1225 (Aab-B, 0.″046 and 1″), J14376−6021 (A-Bab, 0.″94 and 0.″051), and J19246−0839 (A-Bab, 0.″38 and 0.″044).

Of course, the newly detected binaries have to be confirmed through subsequent observations to discard optical pairs, which are unlikely given the small separations, and to start accumulating data to constrain their orbits. Eventually we would like to extend this sample by including stars with intermediate (thick-disk) metallicity, $-1.0 <$ [Fe/H] < -0.4 dex.

[6] See https://hipparcos-tools.cosmos.esa.int/pstex/sect2_01.pdf.

3.4. *TESS Objects of Interest*

Since 2018, HRCam has been used to detect close companions to the TESS objects of interest (TOIs), mostly candidate exohosts. These observations up to 2021.09 and their analysis are published in (C. Ziegler et al. 2020, 2021). Observations made after that date are posted at the EXOFOP-TESS web site[7], but data on the resolved pairs are incomplete there because the main interest was to demonstrate the absence of companions to exohosts. However, new pairs resolved in this campaign are interesting in their own right, for example when they host eclipsing binaries (i.e. are hierarchical systems) or show appreciable orbital motion. We include in Table 1 391 measures of resolved TOIs made between 2021.09 and 2024.0.

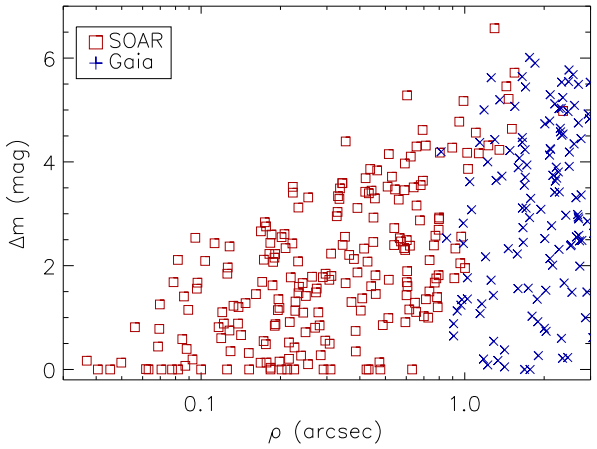

Figure 6. Magnitude difference Δm vs. separation ρ for 220 TOIs resolved at SOAR in 2021–2024 (squares) and for 149 wider pairs also found in GDR3 (crosses).

Many pairs wider than ∼0.″8 are also detected by Gaia. They are marked by the tag 'G' when both components have common parallaxes and/or PMs in GDR3 and by the tag 'g' otherwise (likely unrelated or optical pairs); there are 82 and 67 pairs with G and g tags, respectively, among the TOIs resolved before 2024. This G/g classification based on a quick look at the Gaia astrometry is tentative. The remaining 220 TESS pairs discovered at SOAR are not resolved by Gaia. Figure 6 illustrates the detection of binaries by HRCam (squares) and by GDR3 (crosses); the latter has a comparable dynamic range for pairs wider than ∼0.″8. The Gaia resolution of binaries is expected to improve in the subsequent data releases, eventually down to the diffraction limit of 0.″1 which is still ∼4 times larger than at SOAR.

[7] exofop.ipac.caltech.edu

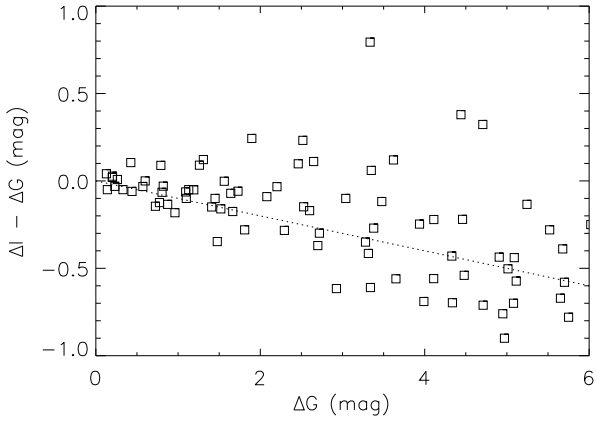

Figure 7. Comparison of the magnitude difference ΔI measured by HRCam with ΔG measured by Gaia for the physical TOI pairs. The dashed line corresponds to $\Delta I = 0.9\Delta G$. The outlier (J21564+2041, HD 208258, 2.″09, $\Delta G = 3.34$, $\Delta I = 4.13$) may have a blue companion.

The TESS-Gaia pairs have been discovered at SOAR independently, offering a blind test of the HRCam data. The comparison is limited here to the 82 physical pairs where Gaia measured both the positions and the magnitude differences ΔG. The Gaia positions match HRCam to within 0.5% of the separation in both radial and tangential directions. The small magnitude differences ΔI agree with ΔG very well (Figure 7), while the larger differences are systematically smaller because the effective wavelength in the I band is longer than in G, and the secondary companions are redder than the primaries. For pairs with $\Delta G < 2$ mag, the rms scatter of $\Delta I - \Delta G$ is 0.11 mag, while for the remaining pairs with larger contrast it is 0.35 mag. These estimates of the photometric accuracy of HRCam are useful because it is the only source of relative photometry for many close pairs, including those with known orbits. Masses of stars derived from the orbits, parallaxes, and relative photometry serve to check stellar evolutionary models.

3.5. *Other New Pairs*

Newly resolved pairs are marked by the tag N in column (15) of Table 1. There are 394 such entries referring to 353 pairs (some pairs were observed more than once), without counting additional 199 wider Gaia pairs discovered at SOAR independently and 67 new pairs with tags A and C. New inner pairs in 37 hierarchical systems are discussed above in Section 3.2, new metal-poor binaries are covered in Section 3.3, and the TOIs in Section 3.4. Other discoveries are reviewed here.

Continuing the work started in 2023, we observed doubly-eclipsing stars discovered by TESS (V. B. Kostov et al. 2022), and resolved seven additional pairs. These are massive stars at distances on

the order of 1 kpc, so only a slow orbital motion is expected. The results of this program, published by S. R. Majewski et al. (2025), are duplicated here in the data tables for completeness.

New pairs are being discovered consistently among reference stars, deemed to be single based on the WDS and Hipparcos and observed for calibrating speckle power spectra of known tight pairs. Here, twelve such binaries are revealed. The tight pair J05422−3032 (HIP 26862) has estimated period of ∼5 yr, and its orbital motion is observed within 1.5 yr.

The large survey of acceleration stars conducted in 2021–2022 resolved 54 pairs (tag A) in addition to several wider pairs also resolved in GDR3 (tag G). This sample is based on the GDR3 astrometry, thus avoiding "obvious" binaries without 5-parameter solutions in GDR3. The newly resolved pairs are either close (below 0.″1) or relatively wide (∼1″) with dim companions. The second group can be contaminated by unrelated (optical) pairs, so we reobserve them after several years to check if the relative motion is consistent with physical binaries. On the other hand, close pairs move fast, and for three of them orbits based on the SOAR data have been computed (J03417−5126, period 3 yr; J10048−3105, 6.9 yr; J14376−1632, 1.7 yr). Acceleration pairs are entered in the WDS with DDs like FR NN.

New subsystems in wide binaries selected from the list by J. J. Andrews et al. (2017) have tag C; 14 of those are present in Table 1. Comments on selected new pairs follow.

J00217−3141 (TYC 6990-325-1) is listed in the WDS as a 0.″8 pair TDS1418 resolved by the Tycho satellite. This pair appears to be spurious because it is not seen by either Gaia or SOAR. Instead, a closer 0.″084 pair Aa,Ab is found. Its estimated period is ∼20 yr.

J04277−3225 (TYC 7038-91-1) is a CPM companion to HIP 20819 located at 56″. The CPM companion is resolved as a 0.″7 binary, while HIP 20819, observed as a reference star, is found to be single.

J04365+2320 is a reference star HIP 21459, found to be double at 0.″17 separation with a large contrast $\Delta I =$ 3.6 mag. The estimated period of this pair is ∼15 yr.

J04558+1502 is another reference star HIP 22913 found to be a 0.″18 double. However, the estimated period is about a century.

J05300+0215 (HD 287952) is a spectroscopic quadruple system detected in the APOGEE spectra by M. Kounkel et al. (2021). It was observed on suggestion by T. Merle and found to be a 0.″30 pair.

J07030−2241 is a 2.″7 Tycho pair TDS4418 according to the WDS. However, we see only a 1.″15 pair with $\Delta I = 3.1$ mag, apparently different from TDS4418. Neither companion is present in GDR3, so we do not know whether the new pair is a chance alignment or not.

J07161−1431 is the reference star HIP 35164, revealed here as a spectacular 0.″06 pair of equal stars. Its period, estimated from the GDR3 parallax of 4.4 mas and separation, is ∼40 yr.

J07547−0421 was observed as TESS object of interest and found to be a triple where the outer 1.″8 pair AB is present in GDR3 and the 0.″26 subsystem BC is new. The GDR3 parallax of 1 mas means that only a very slow motion is expected.

J08418−5304 (HD 74438) is a young compact spectroscopic quadruple in the cluster IC 2391 discovered by T. Merle et al. (2022). The outer period, estimated to be around 5.7 yr from spectroscopy, matches the 0.″034 separation, given the GDR3 parallax of 6.9 mas.

J08599−1546 is a new 0.″04 pair, while the 0.″4 Tycho pair TDS6240 is apparently spurious.

J09266−1626 is the subdwarf star HIP 81661 resolved in 2025 at 0.″1 and showing rapid orbital motion (estimated period ∼7 yr).

J12093−2759 (HIP 59259) is an eclipsing binary QY Hya with a suspected tertiary companion, resolved here at 0.″06. The estimated outer period is ∼4 yr.

J12183−6301 is resolved at 0.″2, while the Tycho pair TDS8311 has a 0.″4 separation. Pending further data, we assume the Tycho pair to be spurious.

J13044−1316 is a resolved quadruple. In addition to the known pairs AB (0.″5) and AC (1.″5), we resolve star B as a 0.″06 equal pair. The Ba,Bb pair is also seen in the 2018 SOAR data, but it was overlooked. Its estimated period is ∼12 yr.

J13130−2430 is clearly resolved as a 0.″04 equal pair, while the 0.″5 pair TDS8731 appears spurious, as many (but not all) similar Tycho doubles.

J14025+0941 (LP 499-23) is revealed as a low-mass triple Bab-C with separations of 0.″08 and 0.″6. The outer pair RAO 309BC has been discovered at the 1.5 m telescope with a resolution insufficient for detecting the inner subsystem; its estimated period is 7 yr. The WDS component A at 930″ (HD 122563) has a similar PM but discordant parallax. For this reason, the triple system should have the WDS code 14035+0935 based on the position of BC, while the optical pair AB should be ignored.

J14562+1745 has been known as a triple system AB-C with separations of 0.″1 and 1.″8; we resolved star C as a 0.″07 pair, so this is a 2+2 quadruple. The 43 yr orbit of AB is known, and the orbit of Ca,Cb can be determined quickly (the estimated period of Ca,Cb is 10 yr).

J15031-4237 is a similar case where the known visual triple Aab-B with separations of 388″ and 0.″1 is

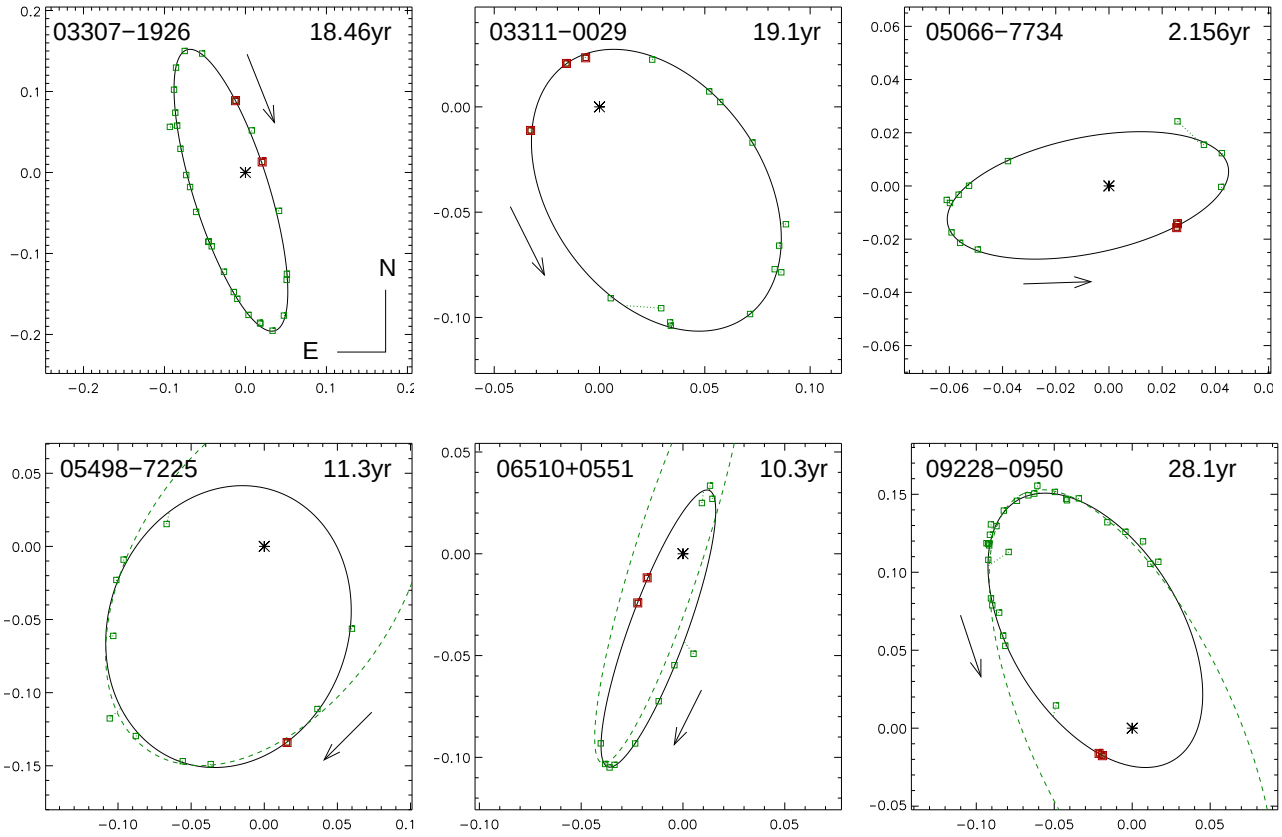

Figure 8. Six new visual orbits with well-constrained elements. In each plot, the ellipse shows the fitted orbit, squares connected to the ellipse are accurate speckle data (bigger red squares for 2024–2025), while visual measures and tentative speckle data are plotted as crosses. The primary component (asterisk) is at coordinate origin, the axis scale is in arcseconds, the orientation is standard (north up, east left). Periods and directions of motion are indicated. Dashed ellipses in the bottom row are substantially revised prior orbits.

turned into a quintuple because its secondary component, L 406-116, contains three stars in a B-Cab arrangement with separations of 0.″9 and 0.″1; the period of Ca,Cb should be around 10 yr. Star B was targeted because GDR3 indicated multi-peak transits. All stars in this system, located at 40 pc from the Sun, are dwarfs of spectral types K and M.

J15053−4104 is a 5th magnitude reference star HIP 73826 resolved tentatively at 18 mas in the y filter by elongation of its power spectrum. Objects observed before and after it do not show such an elongation. However, a RUWE of 1.1 in GDR3 and a constant RV suggest single star, unless this pair is a twin with $\Delta m \sim 0$. The separation implies a period of ∼2 yr, so double lines might be detectable.

J15436−8348 (CPD-83 587), resolved at 0.″06, contains a 1.47 day eclipsing binary detected by both Gaia and TESS.

J15489−5424 (HD 140944) is a known 0.″5 pair FIN 61 where we resolve the secondary component at 0.″05. Despite its small separation, the secondary should have a period on the order of 50 yr because the system is located at ∼1 kpc distance.

J18045−0111 is an M2 dwarf resolved at 0.″16. It also has a CPM companion in GDR3 at 4.″6 separation. The estimated period of Aa,Ab is ∼12 yr.

J18280+0905. The secondary component in the 4.″4 nearby pair, suspected to be a close binary by the large RUWE in GDR3, is resolved here at 0.″11. GDR3 contains four stars with similar parallaxes and PMs located within 27″, so this system is at least quintuple; its components have masses from 0.2 to 0.5 $\mathcal{M}_\odot$.

J18310−5533 is listed in the WDS as two pairs AB and AC with separations of 1.″3 and 3.″8, respectively. However, the pair AB is spurious (not seen by GDR3 and SOAR) and only AC is real. Star C with a large RUWE in GDR3 is resolved here at 0.″12; its estimated period is ∼20 yr.

J19100+1016 is a new 0.″3 pair in the 3″ Tycho double TDT1266. The outer companion B is seen by GDR3, its parallax and PM are discordant with A, so this system is not triple.

J19127−3351 is a triple system HIP 94391 of Bab-C architecture. The WDS component A at 32″ (HIP 94393) is unrelated to BC. Star A has been pointed as a reference and resolved into a 0.″22 pair.

J20311−7508 is yet another case where the 0.″4 Tycho pair TDS2334 turns out to be spurious, while we resolve another 0.″12 binary instead.

J23526+1057 (HIP 117730, 85 Peg) is a naked-eye star resolved at 0.″7 by E. P. Horch et al. (2008) and measured by this team several times using 4 m telescopes. The 0.″06 subsystem Ba,Bb is resolved here for the first time. Its period is estimated to be around 4 yr. The motion of the outer pair AB which has closed down to 0.″23 can be described by a tentative orbit with a 157 yr period.

3.6. *New and Updated Orbits*

The stream of new measures from HRcam allows improvement of known orbits and calculation of new ones. Speckle data gradually replace the less precise and less reliable visual measures, so even well-established visual orbits can be substantially improved if covered by speckle interferometry. The methods of orbit calculation and various caveats are covered in A. Tokovinin (2024b) and we refer to this publication for details such as weights and software tools. Briefly, we fit the orbital elements to the data by the least squares method. Some elements are fixed when they are poorly constrained or degenerate.

Orbit improvement in response to new measures is an almost continuous process. Most corrections are incremental and do not justify publication of updated elements, although the threshold of "significant" corrections is subjective. In some cases, orbits that appeared to be well-defined required dramatic revisions to fit recent measures, and such revisions definitely deserve publication. On the other hand, poorly constrained orbits based on scarce data, useful in their own right, are not reliable and may be substantially revised in the future.

New and corrected orbits resulting from the HRCam data appear in the Information Circulars of the IAU Commission G1 compiled by J.A. Docobo at Observatorio Astronómico Ramón María Aller.[8] These orbits are added to the online ORB6 orbit catalog maintained at USNO[9] (W. I. Hartkopf et al. 2001) and are also featured in this series. Reliable orbits from the Circulars 214–217 are published here, with some adjustments where necessary.

[8] https://www.usc.gal/astro/circularing.html
[9] https://crf.usno.navy.mil/wds-orb6/

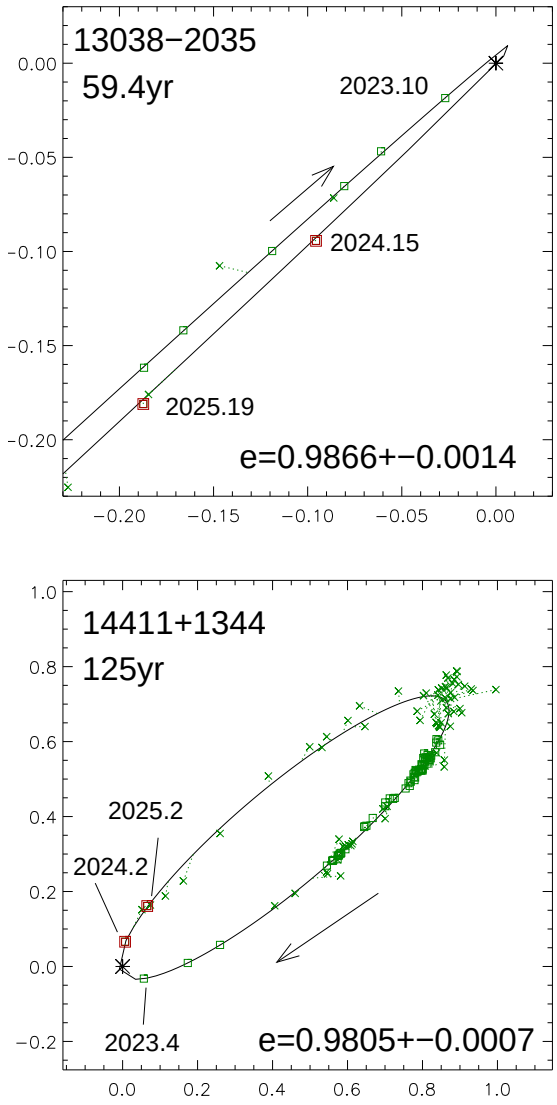

Figure 9. Two new orbits with large and accurately measured eccentricity. The eccentricity and its error are indicated.

For this paper, we selected 202 orbits where all elements are constrained by the data and their errors determined by the least squares fit are meaningful; they are grades A or B in the sense of A. Tokovinin (2024b). The updates of known orbits are deemed substantial or dramatic to warrant publication. In Table 4, each system is identified by its WDS code and the DD (when available), followed by the seven Campbell elements in standard notation. The two rightmost columns contain the provisional orbit grade assigned according to the ORB6 rules and a reference to the most current orbit which has been here improved, when available; the first-time orbits are referenced as SOAR2025. Figure 8 gives illustrative plots of six orbits with accurate elements.

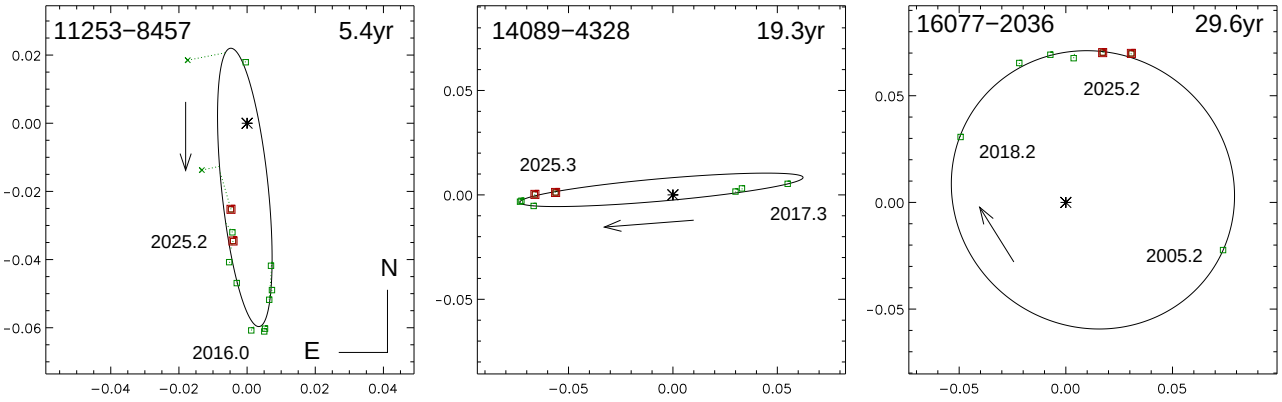

Figure 10. Orbits of three young binaries (see text).

Table 4 contains 10 orbits with eccentricities exceeding 0.9. In two such orbits the eccentricity is fixed because the periastron has not been covered, but the remaining large eccentricities are measured accurately owing to the dense periastron coverage at SOAR; Figure 9 shows two examples. Both are classical visual pairs with relatively long periods that recently passed through the periastron. The first one, J13038−2035 (BU 341), was resolved at 33 mas separation in 2023.10, unresolved in 2023.42, passed through the periastron in 2023.67 (when it was not visible from SOAR), and reappeared again in 2024.16 at $0''.13$, opening up on its 59 yr orbit. The eccentricity of 0.9866 ± 0.0014 is probably the largest reliably measured one, differing from unity by only 0.0134. The second pair J14411+1344 (STF1965AB) passed through the periastron in 1898.4 and in 2023.94; the last periastron was covered at SOAR, constraining the eccentricity to $e = 0.9805 \pm 0.0007$ in this otherwise well-characterized orbit of grade 1 with a period of 125 yr.

In J13038−2035 (HD 113415), the separation between two equal solar-type stars at periastron is only 0.27 au. Twin binaries with orbits of ∼20 au are believed to form via accretion from circumbinary disks accompanied by migration (S. S. R. Offner et al. 2023), which should have damped the eccentricity. Hence, the extreme eccentricity must have been acquired later, when the stars were already on the main sequence and the gas infall stopped. A plausible mechanism is disruption of dynamically unstable triples. Both binaries mentioned here lack known outer companions, supporting the disruption scenario.

Orbits of young binaries are valuable for measuring their masses and testing evolutionary models (M. Simon et al. 2019). With this goal in mind, many young pairs are being monitored at SOAR. Three such orbits are shown in Figure 10. The tight pair J11253−8457 (HIP 55746, BRC 4Aa,Ab) has been discovered at SOAR in 2016 in a survey of the ϵ Cha association (C. Briceño & A. Tokovinin 2017). Its preliminary 9 year circular orbit is updated here to 5.4 year period. The data cover almost two full cycles, but the separation never exceeds 61 mas, so larger telescopes are needed to map the orbit near periastron. Remarkably, ϵ Cha itself was revealed at SOAR as a close triple, and the orbit of its inner subsystem is now known (A. Tokovinin 2023b). The second pair J14089−4328 (HIP 69113, HJ 4653Aa,Ab) of spectral type B9V belongs to the Scorpius-Centaurus (Sco-Cen) association; it has been identified at SOAR in 2017.3, and its first 19.3 yr orbit is determined here. The first orbit of J16077−2036 (BOY 20), also a member of Sco-Cen, is based on the SOAR data, apart from the 2005 discovery measure by H. Bouy et al. (2006). The inclination is fixed at 160° to avoid the degenerate face-on solution. Half of the 29 yr orbit is covered. Two similar M4Ve stars comprising this pair are variable and chromospherically active. The mass sum of 1.14 $\mathcal{M}_\odot$ (using the GDR3 parallax of 6.86±0.07 mas) indicates that these stars will become late-K dwarfs when they settle on the main sequence.

Eight orbits use both positional measures and radial velocities (RVs). In addition to the visual elements in Table 4, we provide in Table 5 the RV amplitudes of the primary and secondary components K_1 and K_2 and the systemic velocity V_0. These parameters, delivered by the joint fit of positions and RVs, are similar but not equal to the published spectroscopic elements. The first three columns repeat the WDS codes, DDs, and periods, and the last column gives references to publications containing the RVs used here. Unpublished RVs measured at the 1.5 m CTIO telescope are referenced as CHIRON (A. Tokovinin 2025b). In the combined orbits, the angles Ω and ω are selected to match both the ascending node and RV of the primary component and the relative positions of the secondary component.

Table 4. Visual Orbits

WDS	Discoverer	P	T	e	a	Ω	ω	i	Grade	Reference[a]
α, δ (2000)	Designation	(yr)	(yr)		(arcsec)	(deg)	(deg)	(deg)		
00111+0513	TOK 869	8.377	2017.893	0.1648	0.1079	111.6	223.9	48.9	2	Tok2023a
		±0.077	±0.132	±0.0109	±0.0019	±1.6	±5.3	±1.5		
00261−1123	YR 4	42.13	2025.963	0.6301	0.2538	49.8	30.2	166.4	3	Msn2023
		±1.25	±0.055	±0.0128	±0.0037	±19.3	±20.8	±7.8		
00417−2446	B 10	171.	2023.428	0.990	0.2523	44.8	69.1	109.0	3	SOAR2025
		±32.	±0.171	fixed	±0.0306	±3.8	±2.3	±3.5		
00460−3043	HDS 100 AB	35.2	2024.054	0.7560	0.1238	33.0	255.2	104.7	3	Tok2023e
		±5.0	±0.054	±0.0245	±0.0129	±1.2	±3.1	±0.9		
01055+1523	GKM9017 Ba,Bb	2.8767	2024.476	0.270	0.0812	54.7	270.2	95.9	3	SOAR2025
		±0.0256	±0.067	±0.082	±0.0056	±1.0	±4.8	±1.2		

[a] Orbit References are provided at https://crf.usno.navy.mil/data_products/WDS/orb6/wdsref.html
(This table is available in its entirety in machine-readable form in the online article.)

Table 5. Combined Spectro-Interferometric Orbits

WDS	Discoverer	P	K_1	K_2	V_0	Reference
α, δ (2000)	Designation	(yr)	(km s^{-1})	(km s^{-1})	(km s^{-1})	
04258+1800	COU2682	45.880	2.43	...	39.96	R. F. Griffin (2012)
		±0.358	±0.07	...	±0.05	
05066−7734	TOK 875	2.156	12.16	12.97	27.46	CHIRON
		±0.001	±0.02	±0.02	±0.01	
11418+0508	TOK 896	3.650	5.73	7.71	18.25	J. Sperauskas et al. (2019)
		±0.005	±0.16	±0.27	±0.14	
13344−2730	TOK 898 Aa,Ab	9.5874	2.03	...	−73.28	D. Barbato et al. (2023)
		±0.0203	±0.01	...	±0.01	
17433+2137	DUQ 1 Aa,Ab	6.9621	9.10	...	23.85	A. Duquennoy et al. (1996)
		±0.0202	±0.12	...	±0.04	
19126+1651	WSI 107 Ca,Cb	6.993	4.61	...	34.09	R. F. Griffin (1979)
		±0.019	±0.25	...	±0.12	
19155−2515	B 430	19.968	12.21	11.55	−26.80	F. C. Fekel (1975)
		±0.031	±1.28	±1.48	fixed	
19512−7248	TOK 697 Aa,Ab	2.9655	11.67	13.82	7.21	CHIRON
		±0.0178	±0.96	±0.85	±0.24	

3.7. *Spurious Pairs*

Some double stars listed in the WDS are actually single. These spurious pairs originate from erroneous visual resolutions or dubious speckle data caused by instrumental artifacts like optical ghosts shown in Figure 11 of TMH10 and in Figure 3 of (A. Tokovinin et al. 2018). Real binary stars, e.g. close ones, also can be resolved spuriously for the same reasons. Identifying spurious pairs will save observing time in the future by eliminating the need to followup and examine these targets. In Table 6 are listed 49 pairs we identify as likely spurious, continuing the clean-up effort from our previous papers. In this table we provide the WDS identifier and DD, the separation, method, and date of the original discovery,

Table 6. Likely Spurious Pairs

WDS	Discoverer	Resolved	Unresolved[a]
00397−2628	HIP 3125	0.25 Spe 2021.7	2023–24 R
02054−0947	LSC 131Aa,Ab	0.2 Spe 2019	2024.9 R
04469−6036	TOK 388AB	0.04 Spe 2014	2014-2024 R,S
09098+1134	CHR 131	0.09 Spe 1986	2024 R,S

[a] Additional indications of the spurious nature of visual pairs: R – no excess noise in GDR3, RUWE<2; L – long estimated period; S – short estimated period or spectroscopic coverage; dm – discrepant magnitude difference.
(This table is available in its entirety in machine-readable form in the online article.)

and the year(s) it has been unresolved in this program. Following that is a code giving other indications supporting the characterization of the double as spurious (see details in A. Tokovinin et al. 2022). In the WDS (B. D. Mason et al. 2001), these pairs are not removed but are given an X code identifying them as a "dubious double" or a "bogus binary".

Among the WDS binaries within 100 pc, 38 pairs were unresolved. All these stars have parallaxes in GDR3. The WDS pairs with multiple prior observations are likely real, but either are too close or have a large contrast. On the contrary, most occultation binaries have been detected only once and never confirmed, so they are suspicious. Another known source of spurious pairs with separations around 0.″5 is the Tycho double star catalog (DD codes TDS and TDT), although several such pairs are confirmed here and one is detected as triple (Section 3.2). WDS J21549−7720 is a real 7.″6 pair detected by both Gaia and SOAR; its separation of 2.″1 measured by Hipparcos (HDS3117AB) is likely explained by wrong interpretation of the modulation produced its focal-plane grating, as happened in a few other cases. The HDS3117AB pair is thus spurious.

4. SUMMARY

This paper reports results of the multi-year campaign of double-star observations with the SOAR speckle camera, continuing previous publications in this series. A total of 7299 observations (both measures and non-resolutions) obtained in 2024 and 2025, as well as previously unpublished earlier data, is the core of this work. We resolved for the first time over 400 pairs, including new inner subsystems in triple stars within 100 pc, metal-poor binaries for future mass measurement, and TOIs. The observations were organized by combining regular time allocations from several projects and the engineering time into a single program. The benefits of this approach are the efficient use of telescope time, the improved time coverage of pairs with fast motion, and the unified data reduction and calibration.

The SOAR speckle data are used in several research projects. Calculation of orbits is the obvious application, leading in turn to the characterization of orbital dynamics in binary and higher-order system and to the measurement of stellar masses. The work by E. H. Vrijmoet et al. (2026) on the orbits of 54 nearby M dwarfs is an excellent illustration of this point. The median semimajor axis of those binaries is 0.″14, and the median orbital period is 6.4 yr. Without a dense coverage (impossible under the classical time allocation scheme), most orbits would have remained undetermined.

The SOAR speckle program complements the Gaia mission (2014–2025). Gaia data are used here for selecting likely binaries, for estimation of periods from separations and parallaxes, and for measurement of masses. The angular resolution of SOAR exceeds that of Gaia by a factor of four, so even in the final Gaia data release, still years ahead, many close binaries will remain unresolved. The SOAR data will help in determination of orbital and astrometric parameters via joint solutions using both Gaia transits and SOAR relative positions. For triple and higher-order systems, Gaia pipelines often fail owing to complex nature of the signals. Future demand for high angular resolution data will be largely driven by Gaia, and SOAR is posed to play a pivotal role here.

ACKNOWLEDGMENTS

We thank SOAR director C. Briceño for allocating some technical time. E.C. and R.A.M acknowledge support form FONDECYT/ANID # 124 0049. R.A.M also acknowledges support from Fondo GEMINI, Astrónomo de Soporte GEMINI-ANID grant # 3223 AS0002. The research of A.T. is supported by the NSFs NOIRLab. Comments by the anonymous referee helped to improve the presentation.

This work used the SIMBAD service operated by Centre des Données Stellaires (Strasbourg, France), bibliographic references from the Astrophysics Data System maintained by SAO/NASA, and the Washington Double Star Catalog maintained at the USNO. This work has made use of data from the European Space Agency (ESA) mission Gaia (https://www.cosmos.esa.int/gaia) processed by the Gaia Data Processing and Analysis Consortium (DPAC, https://www.cosmos.esa.int/web/gaia/dpac/consortium). Funding for the DPAC has been provided by national institutions, in particular the institutions participating in the Gaia Multilateral Agreement.

Facility: SOAR

REFERENCES

Andrae, R., Fouesneau, M., Sordo, R., et al. 2023, A&A, 674, A27, doi: 10.1051/0004-6361/202243462

Andrews, J. J., Chanamé, J., & Agüeros, M. A. 2017, MNRAS, 472, 675, doi: 10.1093/mnras/stx2000

Barbato, D., Ségransan, D., Udry, S., et al. 2023, A&A, 674, A114, doi: 10.1051/0004-6361/202345874
Bouy, H., Martín, E. L., Brandner, W., et al. 2006, A&A, 451, 177, doi: 10.1051/0004-6361:20054252
Briceño, C., & Tokovinin, A. 2017, AJ, 154, 195, doi: 10.3847/1538-3881/aa8e9b
Clark, C. A., van Belle, G. T., Horch, E. P., et al. 2024, AJ, 167, 56, doi: 10.3847/1538-3881/ad0bfd
Duquennoy, A., Tokovinin, A. A., Leinert, C., et al. 1996, A&A, 314, 846
Faes, D. M., Tokovinin, A., Vieira, T., et al. 2018, in Society of Photo-Optical Instrumentation Engineers (SPIE) Conference Series, Vol. 10703, Adaptive Optics Systems VI, ed. L. M. Close, L. Schreiber, & D. Schmidt, 107033C, doi: 10.1117/12.2312205
Fekel, F. C. 1975, AJ, 80, 844, doi: 10.1086/111820
Gaia Collaboration, Brown, A. G. A., Vallenari, A., et al. 2021a, A&A, 649, A1, doi: 10.1051/0004-6361/202039657
Gaia Collaboration, Brown, A. G. A., Vallenari, A., et al. 2016, A&A, 595, A2, doi: 10.1051/0004-6361/201629512
Gaia Collaboration, Smart, R. L., Sarro, L. M., et al. 2021b, A&A, 649, A6, doi: 10.1051/0004-6361/202039498
Griffin, R. F. 1979, The Observatory, 99, 36
Griffin, R. F. 2012, Journal of Astrophysics and Astronomy, 33, 29, doi: 10.1007/s12036-012-9137-5
Hartkopf, W. I., Mason, B. D., & Worley, C. E. 2001, AJ, 122, 3472, doi: 10.1086/323921
Hartkopf, W. I., Tokovinin, A., & Mason, B. D. 2012, AJ, 143, 42, doi: 10.1088/0004-6256/143/2/42
Hartman, Z. D., van Belle, G., Lépine, S., Everett, M. E., & Medan, I. 2025, AJ, 170, 91, doi: 10.3847/1538-3881/add7d3
Horch, E. P., van Altena, W. F., Cyr, Jr., W. M., et al. 2008, AJ, 136, 312, doi: 10.1088/0004-6256/136/1/312
Horch, E. P., van Altena, W. F., Demarque, P., et al. 2015, AJ, 149, 151, doi: 10.1088/0004-6256/149/5/151
Horch, E. P., Casetti-Dinescu, D. I., Camarata, M. A., et al. 2017, AJ, 153, 212, doi: 10.3847/1538-3881/aa6749
Horch, E. P., Tokovinin, A., Weiss, S. A., et al. 2019, AJ, 157, 56, doi: 10.3847/1538-3881/aaf87e
Horch, E. P., Broderick, K. G., Casetti-Dinescu, D. I., et al. 2021, AJ, 161, 295, doi: 10.3847/1538-3881/abf9a8
Howell, S. B., Scott, N. J., Matson, R. A., et al. 2021, Frontiers in Astronomy and Space Sciences, 8, 10, doi: 10.3389/fspas.2021.635864
Janson, M., Hormuth, F., Bergfors, C., et al. 2012, ApJ, 754, 44, doi: 10.1088/0004-637X/754/1/44
Katz, D., Sartoretti, P., Guerrier, A., et al. 2023, A&A, 674, A5, doi: 10.1051/0004-6361/202244220
Kostov, V. B., Powell, B. P., Rappaport, S. A., et al. 2022, ApJS, 259, 66, doi: 10.3847/1538-4365/ac5458
Kounkel, M., Covey, K. R., Stassun, K. G., et al. 2021, AJ, 162, 184, doi: 10.3847/1538-3881/ac1798
Lester, K. V., Howell, S. B., Matson, R. A., et al. 2023, AJ, 166, 166, doi: 10.3847/1538-3881/acf563
Lindegren, L., Klioner, S. A., Hernández, J., et al. 2021, A&A, 649, A2, doi: 10.1051/0004-6361/202039709
Majewski, S. R., Davidson Jr., J. W., Wilson, R. F., et al. 2025, arXiv e-prints, arXiv:2511.07554. https://arxiv.org/abs/2511.07554
Mann, A. W., Dupuy, T., Kraus, A. L., et al. 2019, ApJ, 871, 63, doi: 10.3847/1538-4357/aaf3bc
Mason, B. D., & Hartkopf, W. I. 2026, AJ, 171, 149, doi: 10.3847/1538-3881/ae3748
Mason, B. D., Hartkopf, W. I., Gies, D. R., Henry, T. J., & Helsel, J. W. 2009, AJ, 137, 3358, doi: 10.1088/0004-6256/137/2/3358
Mason, B. D., Tokovinin, A., Mendez, R. A., & Costa, E. 2023, AJ, 166, 139, doi: 10.3847/1538-3881/acedaf
Mason, B. D., Wycoff, G. L., Hartkopf, W. I., Douglass, G. G., & Worley, C. E. 2001, AJ, 122, 3466, doi: 10.1086/323920
McAlister, H. A., Mason, B. D., Hartkopf, W. I., & Shara, M. M. 1993, AJ, 106, 1639, doi: 10.1086/116753
Mendez, R. A., Clavería, R. M., & Costa, E. 2021, AJ, 161, 155, doi: 10.3847/1538-3881/abdb28
Mendez, R. A., Tokovinin, A., Costa, E., & Dirk, M. 2025, AJ, 169, 226, doi: 10.3847/1538-3881/adbbb4
Merle, T., Hamers, A. S., Van Eck, S., et al. 2022, Nature Astronomy, 6, 681, doi: 10.1038/s41550-022-01664-5
Mitrofanova, A., Dyachenko, V., Beskakotov, A., et al. 2021, AJ, 162, 156, doi: 10.3847/1538-3881/ac1a78
Offner, S. S. R., Moe, M., Kratter, K. M., et al. 2023, in Astronomical Society of the Pacific Conference Series, Vol. 534, Protostars and Planets VII, ed. S. Inutsuka, Y. Aikawa, T. Muto, K. Tomida, & M. Tamura, 275, doi: 10.48550/arXiv.2203.10066
Penoyre, Z., Belokurov, V., & Evans, N. W. 2022, MNRAS, 513, 5270, doi: 10.1093/mnras/stac1147
Powell, B. P., Kostov, V. B., & Tokovinin, A. 2023, MNRAS, 524, 4296, doi: 10.1093/mnras/stad2065
Raghavan, D., McAlister, H. A., Henry, T. J., et al. 2010, ApJS, 190, 1, doi: 10.1088/0067-0049/190/1/1
Recio-Blanco, A., de Laverny, P., Palicio, P. A., et al. 2023, A&A, 674, A29, doi: 10.1051/0004-6361/202243750
Simon, M., Guilloteau, S., Beck, T. L., et al. 2019, ApJ, 884, 42, doi: 10.3847/1538-4357/ab3e3b
Sperauskas, J., Deveikis, V., & Tokovinin, A. 2019, A&A, 626, A31, doi: 10.1051/0004-6361/201935346

Tokovinin, A. 2012, AJ, 144, 56, doi: 10.1088/0004-6256/144/2/56
Tokovinin, A. 2018a, PASP, 130, 035002, doi: 10.1088/1538-3873/aaa7d9
Tokovinin, A. 2018b, AJ, 155, 160, doi: 10.3847/1538-3881/aab102
Tokovinin, A. 2021, Universe, 7, 352, doi: 10.3390/universe7090352
Tokovinin, A. 2023a, AJ, 165, 180, doi: 10.3847/1538-3881/acc464
Tokovinin, A. 2023b, AJ, 165, 165, doi: 10.3847/1538-3881/acbf32
Tokovinin, A. 2023c, AJ, 165, 160, doi: 10.3847/1538-3881/acbe42
Tokovinin, A. 2024a, AJ, 168, 125, doi: 10.3847/1538-3881/ad6153
Tokovinin, A. 2024b, AJ, 168, 190, doi: 10.3847/1538-3881/ad72e5
Tokovinin, A. 2025a, AJ, 169, 124, doi: 10.3847/1538-3881/ada3c6
Tokovinin, A. 2025b, AJ, 170, 143, doi: 10.3847/1538-3881/adee23
Tokovinin, A. 2026a, AJ, 171, 109, doi: 10.3847/1538-3881/ae2fe6
Tokovinin, A. 2026b, ApJ, 998, 151, doi: 10.3847/1538-4357/ae3682
Tokovinin, A., Cantarutti, R., Tighe, R., et al. 2016a, PASP, 128, 125003, doi: 10.1088/1538-3873/128/970/125003
Tokovinin, A., Cantarutti, R., Tighe, R., et al. 2010a, PASP, 122, 1483, doi: 10.1086/657903
Tokovinin, A., Mason, B. D., & Hartkopf, W. I. 2010b, AJ, 139, 743, doi: 10.1088/0004-6256/139/2/743
Tokovinin, A., Mason, B. D., & Hartkopf, W. I. 2014, AJ, 147, 123, doi: 10.1088/0004-6256/147/5/123
Tokovinin, A., Mason, B. D., Hartkopf, W. I., Mendez, R. A., & Horch, E. P. 2015, AJ, 150, 50, doi: 10.1088/0004-6256/150/2/50
Tokovinin, A., Mason, B. D., Hartkopf, W. I., Mendez, R. A., & Horch, E. P. 2016b, AJ, 151, 153, doi: 10.3847/0004-6256/151/6/153
Tokovinin, A., Mason, B. D., Hartkopf, W. I., Mendez, R. A., & Horch, E. P. 2018, AJ, 155, 235, doi: 10.3847/1538-3881/aabf8d
Tokovinin, A., Mason, B. D., Mendez, R. A., & Costa, E. 2022, AJ, 164, 58, doi: 10.3847/1538-3881/ac78e7
Tokovinin, A., Mason, B. D., Mendez, R. A., & Costa, E. 2024, AJ, 168, 28, doi: 10.3847/1538-3881/ad4d56
Tokovinin, A., Mason, B. D., Mendez, R. A., Costa, E., & Horch, E. P. 2020, AJ, 160, 7, doi: 10.3847/1538-3881/ab91c1
Tokovinin, A., Mason, B. D., Mendez, R. A., et al. 2021, AJ, 162, 41, doi: 10.3847/1538-3881/ac00bd
Tokovinin, A., Mason, B. D., Mendez, R. A., Horch, E. P., & Briceño, C. 2019, AJ, 158, 48, doi: 10.3847/1538-3881/ab24e4
Torres, G., Schaefer, G. H., Monnier, J. D., et al. 2022, ApJ, 941, 8, doi: 10.3847/1538-4357/ac9d8d
Vrijmoet, E. H., Tokovinin, A., Henry, T. J., et al. 2022, AJ, 163, 178, doi: 10.3847/1538-3881/ac52f6
Vrijmoet, E. H., Tokovinin, A., Henry, T. J., et al. 2026, AJ, 171, XXX, doi: TBD
Ziegler, C., Tokovinin, A., Briceño, C., et al. 2020, AJ, 159, 19, doi: 10.3847/1538-3881/ab55e9
Ziegler, C., Tokovinin, A., Latiolais, M., et al. 2021, AJ, 162, 192, doi: 10.3847/1538-3881/ac17f6

Table 7. List of Calibrator Binaries

WDS	DD	HIP	N	ρ ($''$)	Δm (mag)	Mod.	$\sigma_{\rm tan}$ (mas)	$\sigma_{\rm rad}$ (mas)
00098−3347	SEE 3	794	12	0.78	1.47	2	1.7	2.1
00522−2237	STN 3AB	4072	31	1.99	0.78	1	2.0	3.5
01024+0504	HDS 135AB	4849	11	0.71	1.36	2	3.0	1.4

NOTE—(This table is available in its entirety in machine-readable form in the online article.)

APPENDIX

A. SOAR CALIBRATORS

In this Appendix, we give the updated set of the SOAR calibrator binaries and the models of their motion. Table 7 lists the WDS codes, DDs, and Hipparcos numbers of 86 binaries. The following columns contain the number of runs N (multiple observations in one run, if available, are averaged and considered as single measure), the mean separation ρ, and the approximate magnitude difference Δm. The linear and orbital models are denoted by 1 and 2, respectively. The last two columns give the rms residuals from the models in tangential and radial directions. As noted, a few deviant (by more than 2.5σ) measures of some calibrators were discarded.

Table 8. Linear Models

WDS	t_0 (JY)	θ_0 (°)	$\dot\theta$ (° yr^{-1})	ρ_0 ($''$)	$\dot\rho$ ($''$ yr^{-1})
00522−2237	2019.989	241.015	−0.243	1.9832	0.0005
01037−3024	2019.193	236.870	−0.106	0.8563	0.0022
05019−7638	2020.356	154.993	0.634	0.8251	0.0037
05508−2907	2019.420	329.875	0.087	2.1657	0.0019
06425−4234	2019.055	194.781	0.151	2.3363	−0.0005
08461+0748	2020.828	339.942	0.033	2.7972	0.0016
09125−4337	2019.517	280.826	−0.009	2.8983	0.0037
13142−1634	2021.287	259.584	−0.029	1.6688	0.0112
15308−0746	2021.109	342.180	0.883	1.0561	0.0024
15428−1601	2020.740	110.771	0.159	1.5931	−0.0102
17315−4156	2021.636	37.106	−0.160	1.4509	0.0040
19426−5901	2020.536	148.749	−0.119	2.4728	0.0099
22152−0535	2018.233	280.213	0.015	0.6954	0.0001

The slow motion of a wide binary can be represented by linear functions of time in polar coordinates (ρ, θ):

$$\theta(t) = \theta_0 + \dot\theta\ (t - t_0), \tag{A1}$$

$$\rho(t) = \rho_0 + \dot\rho\ (t - t_0), \tag{A2}$$

where t_0 is the mean time of observation. These equations describe a spiral trajectory. Fragment of a spiral is a better match to an orbital segment than a linear trajectory in rectangular coordinates, with the same number of 5 free parameters (for a circular face-on orbit, the spiral is accurate). The choice of t_0 ensures that the offsets and slopes are statistically independent. Parameters of the linear models for 13 calibrators are given in Table 8.

Table 9 lists the orbital elements of the remaining 73 pairs, in standard notation. The last column gives reference to the catalog orbits used as templates (the reference codes are available in ORB6). Only the elements (T, a, Ω) were fitted to the SOAR data (including also Hipparcos and GDR3 positions when available) if the templates are adequate. Otherwise, all elements were slightly corrected using all available data with suitable weights (A. Tokovinin 2024b), and then the 3 elements were fitted to the SOAR data only; such cases are marked by asterisks after the references. Cases when corrections of the template orbits are substantial are marked by single asterisks in the reference column. We caution that the orbits in Table 9 are specially adjusted to match the SOAR data and are not necessarily the best orbits of these binaries in general sense (although they might be better than current catalog orbits). There are five overlaps with orbits in Table 4 (WDS codes 04199+1631, 10426+0335, 14489+0557, 16044−1122, and 23100−4252); Table 4 should be preferred over the orbital models of the calibrators.

Table 9. Orbital Elements

WDS	P (yr)	T (JY)	e	a ($''$)	Ω ($^\circ$)	ω ($^\circ$)	i ($^\circ$)	Reference[a]
00098−3347	295.106	1978.59	0.7668	0.9242	275.70	71.15	32.83	Tok2024a*
01024+0504	28.320	2002.70	0.6721	0.4616	268.23	22.08	144.79	Tok2015c*
01084−5515	289.600	1920.48	0.5970	1.1863	24.44	292.20	71.20	Lin2019a
01158−6853	85.137	2001.26	0.0396	1.0868	140.67	132.65	31.08	Tok2024a
01262−6751	374.193	1951.95	0.8491	1.1875	135.82	347.65	47.47	Izm2019

[a] Orbit References are provided at https://crf.usno.navy.mil/data_products/WDS/orb6/wdsref.html. The asterisks mark references where more than three elements are adjusted. Substantial orbit revisions have single asterisks in the Reference column.

(This table is available in its entirety in machine-readable form in the online article.)